INTERCELL CURRENTS IN ASSEMBLY OF MODULES: QUALITY CONTROL CONSIDERATIONS

C. J. GABRIEL*, P. A. MOSIER-BOSS and S. SZPAK
Naval Ocean Systems Center, San Diego, CA 92152-5000 (U.S.A.)
J. J. SMITH
Department of Energy, Washington, DC 20545 (U.S.A.)

(Received February 20, 1990; in revised form April 27, 1990)

Summary

Quality control considerations in battery fabrication with regard to intercell currents in an assembly of modules of thin cell, bipolar plate design connected in parallel electrically and in series hydraulically, are examined. The effects on battery performance of a statistical distribution in the parameters of the porous cathode structure, as well as unequal compression/expansion of the module and unequal number of cells in modules, are investigated. The discharge performance of modules with defective cells is also considered. Modeling methods are general; however, the examples used to illustrate pertain to the $Li/SOCl_2$ system.

1. Introduction

The efficient operation of equipment designed for electrochemical processing, including energy conversion devices, often requires the installation of a common electrolytic path. There are numerous advantages associated with this approach, *viz.*, bipolar cell construction, controlled supply of reactants and removal of products, as well as a reliable means of thermal management. These advantages, however, are partially off-set by the parasitic shunting action of the intercell currents. In practice, these currents not only reduce the power output but often affect the structural integrity of battery functional elements [1].

In a previous communication [2] we concluded that in well designed modules of thin cell, bipolar plate design, connected electrically in parallel and hydraulically in series, an increase in their number does not inherently increase the imbalance in intercell or nodal currents. However, in an

*Author to whom correspondence should be addressed.

0378-7753/90/$3.50

assembly of modules with one or more defective cells, or with a sufficiently large variation among the cell functional elements, a situation arises which substantially reduces the battery lifetime and, on occasion, may lead to catastrophic events. In this communication, we examine, in general terms, the effect of abnormal deviation from the average value of pertinent parameters on the performance characteristics of a multi-module battery.

2. Battery fabrication

Three areas require particularly close attention during the design phase of a battery. The first relates to maximizing the extractable energy for an *a priori* given power output. The second involves minimizing the time and energy required to activate the battery or the power needed to circulate the electrolyte. The third area of concern is thermal management to realize a high power output design or to maintain the integrity of cell functional elements during operation for extended periods of time.

To minimize the power losses, a low discharge current density arrangement requiring a high potential is desired. This, in turn, requires a large number of cells in each module with several of these modules connected in parallel. To maximize the extractable energy density a compact design is needed, *i.e.*, a thin cell design [3]. As a rule, the amount of electroactive material, hence the cell thickness and area, is a function of the required discharge time, usually expressed as the time needed to reach an *a priori* specified cell/battery voltage. Cells as thin as 0.044 cm can be fabricated [4]. Of course, fabricating the very thin cells places special demands on the manufacturing and assembly process.

2.1. Fabrication sequence

A typical module fabrication sequence is summarized in the form of a block diagram in Fig. 1. The cell functional elements, *e.g.*, positive and negative electrode structures, are first fabricated. Then, other components

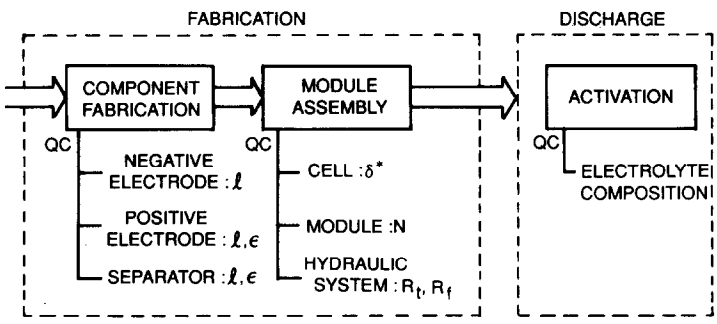

Fig. 1. Block diagram indicating the fabrication sequence for module/battery assembly and QC requirements. l, thickness; N, number of cells; R_f and R_t, feed line and fill tube resistances, respectively; δ^*, electrode separation; ϵ, porosity.

such as separators, bipolar plates, current collectors, etc., are cut to size. The assembly process consists of stacking the cells and compressing the stack to the designed thickness. Finally, means for battery activation or electrolyte circulation are provided to complete the process of module assembly.

2.2. Quality control (QC) measures

Quality control measures are closely connected with fabrication steps and the dynamics of the cell/module operation. Thus, in the course of component fabrication, not only must the amount of stored electroactive material be controlled but also the geometrical constraints of the porous structure. The control of the purity and amount of the electroactive material present no special problems. On the other hand, the control of geometrical constraints is a serious and, as yet, unresolved problem. Porous electrodes are usually made by sintering or by a combination of rolling and/or pressing of the particles comprising the electrodes. Thus, the fabrication of porous electrodes incurs statistically spread deviations in structural parameters such as specific surface area, porosity, tortuosity, particle and pore size. According to Dunning [6], the description of the interplay between elementary processes associated with the charge transfer and the geometry of the electrode structure requires consideration of three averages: an average over the volume of the electrolyte phase in pores, an average over the interfacial area between the electrode matrix and electrolyte, and an average over the cross section exposing electrode matrix and pores.

It is not our purpose to suggest or promote any particular form of QC activities; rather to indicate the need for such activities and discuss the consequences of their absence in terms of power loss [5], thermal management, and the integrity of functional elements. The relevant properties are indicated in Fig. 1 alongside the fabrication sequence.

3. Electric circuit analog

The characteristic features of an operating electrochemical cell can be, and are often, simulated by an electric circuit analog. Examples with regard to battery technology are numerous [7].

3.1. Assumptions and definitions

In the present discussion, we retain all of the definitions and assumptions of refs. 1 and 2. In particular:

(i) an intercell current is an ionic current that originates in one cell and terminates in another;

(ii) the current distribution is adequately simulated by an electric circuit analog, Fig. 2;

(iii) the phenomenological coefficients associated with the ionic current are replaced by resistances;

(iv) the potentials in the electrolyte phase at the entrance port to the cell, Φ_i, are uniform;

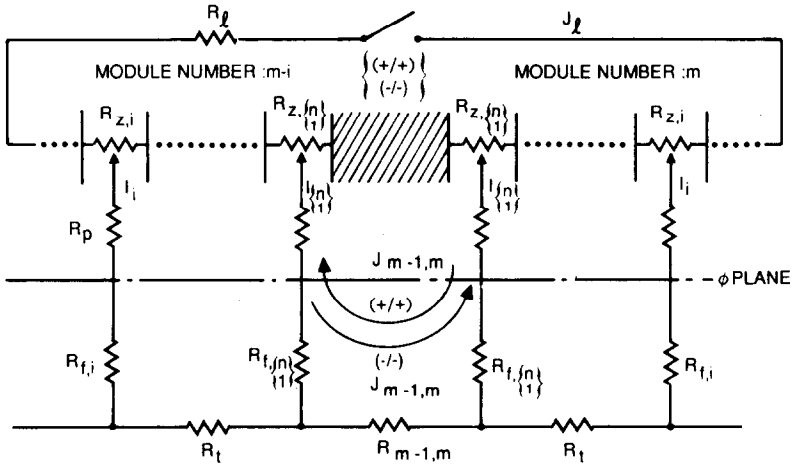

Fig. 2. Module and module/module coupling representation by an electric circuit analog. J_i, circulating current; I_i, intercell current; Φ, potential at manifold inlet; R_f, manifold feed resistor; R_t, equivalent feed tube resistor; R_z, internal cell impedance. Both (+/+) and (—/—) interfaces are indicated.

(v) the bipolar plates are equipotential;

(vi) the intercell current, I_i, is equal to the difference between circulating currents, *i.e.*, $I_i = J_i - J_{i-1}$;

(vii) circulating currents at the coupling interfaces between modules have finite values while those at battery terminal cells are zero.

The replacement of the phenomenological coefficients by the lumped resistances implies uniform current distributions on the cross sections of the associated segments.

3.2. *The* λ *parameter*

An analysis of the electric circuit analog, representing a single module, is given in ref. 1, while that for an assembly of modules is given in ref. 2. In both cases, it is convenient to introduce the parameter λ. This parameter depends on the battery design, the properties of the electrolyte employed, and the kinetics of the charge transfer reaction(s) occurring within the confines of the porous structures of the electrodes. For the special case, where all cell parameters are uniform throughout the modules, the expression for the intercell currents can be obtained in a closed form [1], with λ given by eqn. (1)

$$\lambda = 1 + X + \sqrt{X(2 + X)} \tag{1}$$

in which $X = (R_t + R_z)/2R_f^*$ where $R_f^* = R_f + R_p - R_z\sigma^2/\sigma_a\sigma_c$. Physically, the λ parameter indicates the ratio of intercell currents in adjacent cells, *i.e.*, I_{i+1}/I_i. In particular, for modules with large numbers of cells, *e.g.*, $N > 50$, $I_{i+1}/I_i = \lambda^{-1}$ as $i \to 1$, and $I_{i+1}/I_i = \lambda$ as $i \to N$ (ref. 1, eqns. (36) and (37)).

A cursory analysis of eqn. (1) reveals that the constancy of the λ parameter is assured only if the devices are capable of a steady-state

operation (this implies the constancy of power output and not of electrochemical processes), *e.g.*, fuel cells and electrolyzers, providing, however, that the inert structures are not modified by passivation or corrosion. In other cases, its constancy cannot be assumed. The time dependence of the λ parameter is specific for a given battery system and can be, at least qualitatively, assessed with the aid of the electric circuit analog, Fig. 3. Thus, the R_t can be regarded as being constant throughout the discharge period, the R_z are functions of the transferred charge, and the R_p are determined by the geometry of the entrance port and the nature of the electrochemical system.

In analogy with the special case, eqn. (1), we can define the parameter ${}^{(m)}\lambda_i$, eqn. (2):

$$ {}^{(m)}\lambda_i = 1 + {}^{(m)}X_i + \sqrt{{}^{(m)}X_i(2 + {}^{(m)}X_i)} \qquad (2) $$

where ${}^{(m)}X_i$ is defined similarly to X (*vide supra*), except that here the parameters R_t, R_z and R_f^* are identified with the i-th cell in the m-th module. In contrast to the special case, eqn. (1), here, the ${}^{(m)}\lambda_i$ parameter characterizes the time dependent behavior of groups of cells, as they degrade in the course of battery discharge, rather than a complete module.

As illustrated in Fig. 4(a), initially the λ parameter is statistically uniform throughout the multimodule battery. Its numerical value ranges between 1.16 and 1.18 and the distribution among cells reflects the statistical variation of the functional elements. However, as the battery discharges, the individual cell functional elements undergo changes, principally due to the contribution of intercell currents. The groups of cells at

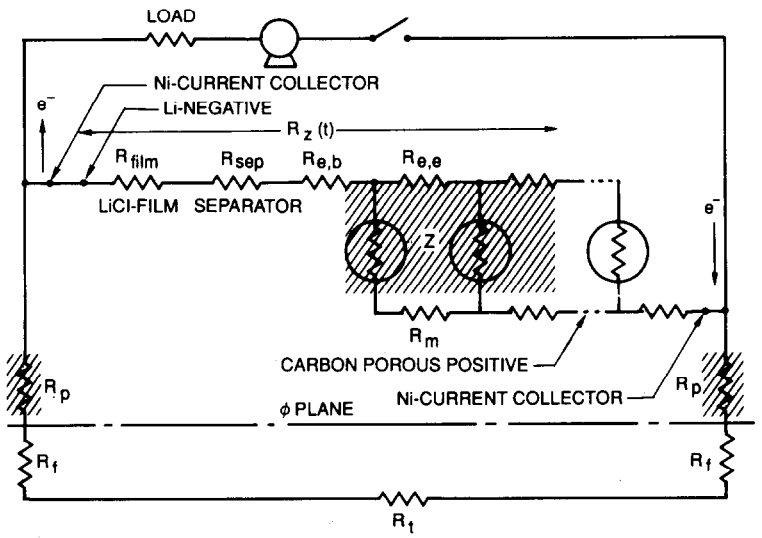

Fig. 3. An electric circuit analog representation of an operating $Li/SOCl_2$ cell. Shaded areas indicate the locations of the time dependent circuit elements relevant to the computed results.

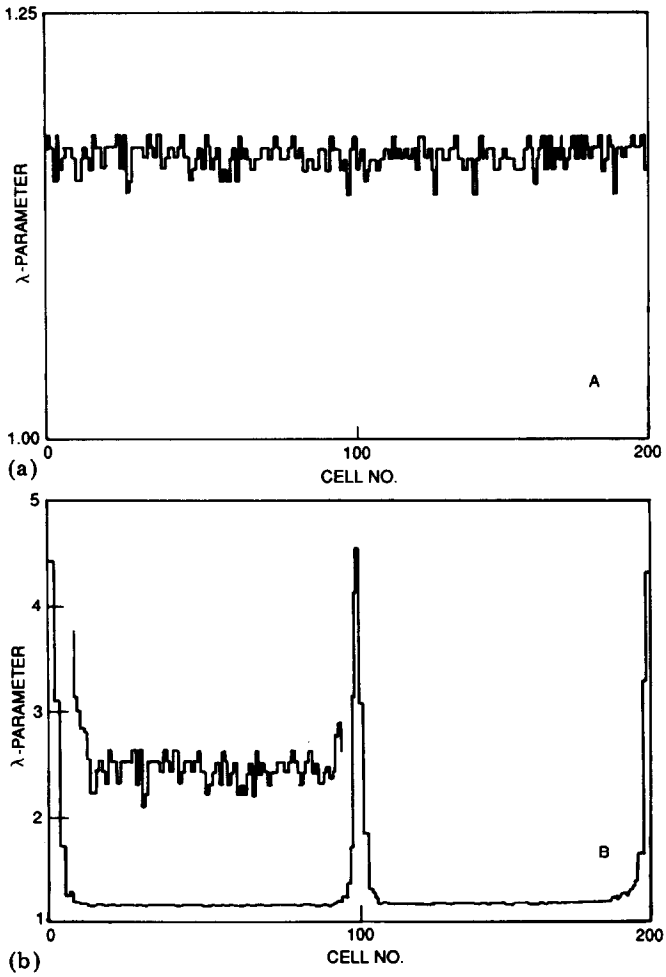

Fig. 4. The time evolution of λ parameter calculated for each cell in an assembly of four, fifty-cell modules for the input data listed in Table 1, with N_s = 10.0. (a) Initial distribution; (b) distribution after 288 s of battery discharge. The insert is the expansion, to the same scale as in (a), of the interface between the first and second modules.

the negative end of modules are substantially affected, as seen in Fig. 4(b). It is noted that changes in the λ parameter, and the behavior of these cells, should be examined in conjunction with Fig. 5(a) and (b), where it is also seen that changes have occurred at the module negative end.

3.3. Quality control (QC) points

The cell internal resistance is, first and foremost, a function of the discharge rate and duration. To analyze the time dependence it is convenient to represent the cell processes in terms of components of an electric circuit analog. The situation within a single cell is illustrated in Fig. 3. The

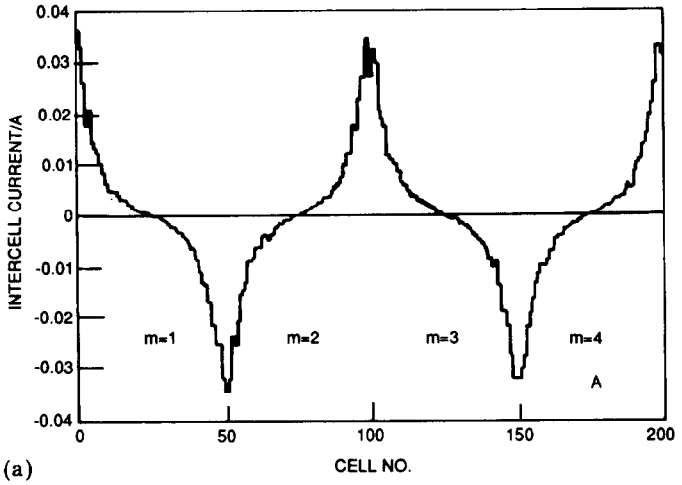

(a)

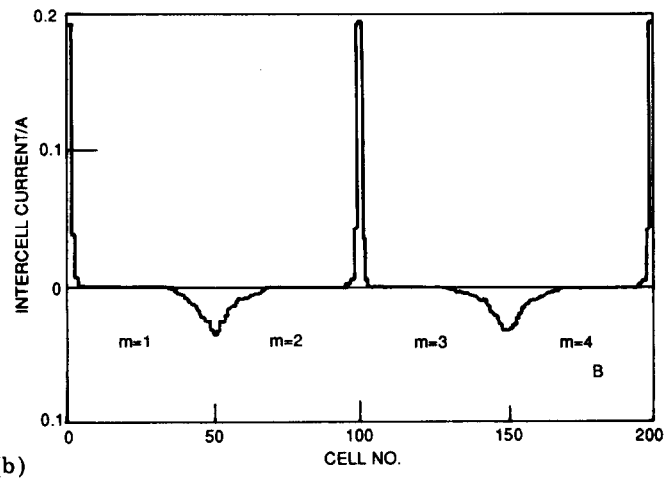

(b)

Fig. 5. Time evolution of intercell currents. Conditions as in Fig. 4.

time-dependent component is principally located within the porous structure of the positive electrode where a precipitation of the solid phase occurs, *i.e.*, in the shaded area. The rate of change of the cell internal resistance is a function of the initial porosity and the rate at which the reaction front penetrates the electrode structure. This rate, expressed here by the combination of an effective electrode separation, δ^*, and the time-dependent electrolyte conductivity, in general, varies during the cell discharge in a complex way [2]. We shall not dwell on this relationship other than to indicate which input parameters are affected and their physical significance.

The statistical variation in R_z arising from unequal compression of individual cells is here associated with both a variation of the cell porosity, ϵ_z, and a variation of the effective cell electrode spacing, δ^*, (see eqn. (13),

ref. 1 and eqn. (15), ref. 2). The cell porosity is derived from the distribution of random variables, y, where y is chosen from the binomial distribution having a probability of success $(\epsilon_{z,n} - \epsilon_{min})/(\epsilon_{max} - \epsilon_{min})$, and a number of trials, N_s, according to the relationship $y/N_s = (\epsilon_z - \epsilon_{min})/(\epsilon_{max} - \epsilon_{min})$. This choice produces a distribution for $\epsilon_{min} < \epsilon_z < \epsilon_{max}$ having a mean $\eta_\epsilon = \epsilon_{z,n}$ and a standard deviation $\sigma_\epsilon = \sqrt{(\epsilon_{z,n} - \epsilon_{min})(\epsilon_{max} - \epsilon_{z,n})/N_s}$. The variation of δ^* is introduced as an arbitrarily chosen percentage deviation from the design point for each module. In this communication we limit the discussion to the above mentioned variation in cell impedance and the occurrence of different numbers of cells in the module of multimodule assemblies — the latter arising from an operator error, which is a rare but not unheard of incident in assembling modules containing 100 or more cells.

The time dependence, $R_z(t)$, associated with the dynamics of the battery discharge, is introduced via the rate of change of the cathode conductance, $\kappa_c(t)$, eqn. (3):

$$\kappa_c(t) = \frac{w\kappa\epsilon_z}{1 + (Q(t)/Q)^{\xi_c}} \tag{3}$$

with $Q(t) = \int_0^t I\,dt$ and $Q = w\tau NU/(MR_1 + NR_{z,n})$, where w is the deficiency factor [1]. Here $Q(t)$ is the actual amount of charge transferred to the positive electrode within the time period t, while Q represents the charge that would be transferred within the battery lifetime, τ, under conditions of no parasitic current flow. The adjustable parameter, ξ_c, is related to the morphology of the solid reaction products; here, it is chosen so that the calculated module discharge characteristics approximate observed behavior. The time variation of the feed tube resistance, R_f, affects the operation of a battery and the distribution of intercell currents, but is essentially a design factor rather than a QC issue. The time dependency and statistical variation of R_f is included here in a manner reported in ref. 2.

3.4. Construction of solution

Figure 6 shows a flowchart of the solution program used to calculate the intercell currents within an assembly of modules. First, the geometry and physical properties of the module(s) are defined. The system parameters include the number of modules (maximum of 5), the number of cells per module (maximum of 90), porosity-fineness of the cathodes, cathode use factor, anode reversed current factor, and load resistance, as defined in ref. 2. The cell and feed tube porosities are assigned from the same distribution, as described in Section 3.3, using a random number generator. The porosities were chosen from the range 0.3 - 0.9, corresponding to limitations imposed by heat evolution [8] and practical considerations of cell construction. In the case of deficient modules, the number, location, and deficiency factor of the affected cells are defined. In these calculations, the effective electrode spacing is assumed to be the same for each cell within the module.

Once the system parameters have been established, the starting cell and feed tube conductivities are calculated and the computations for each time

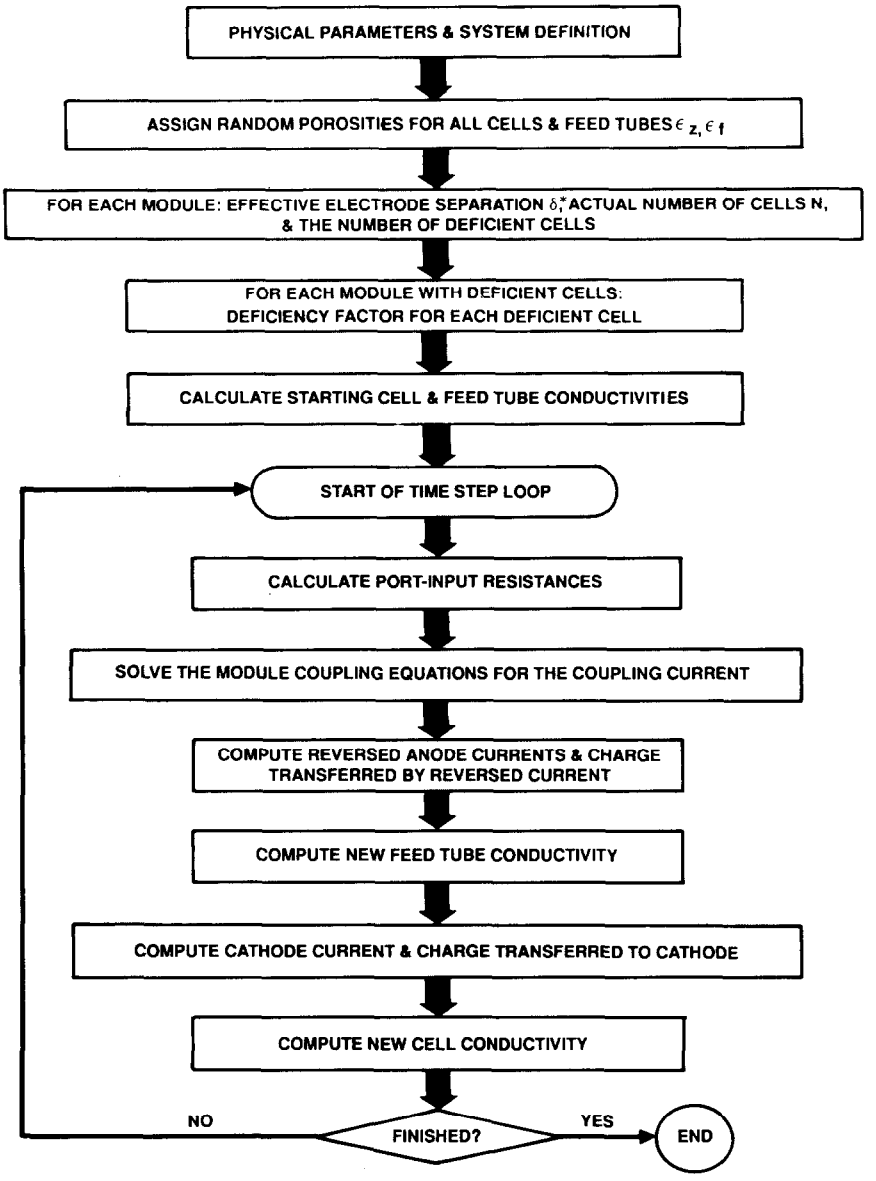

Fig. 6. Flow chart for calculation of characteristics of the multi-module battery discharge.

step are started. Within the time loop the port input resistances are calculated (eqn. (1), ref. 1), and the tridiagonal banded matrix for each module's loop currents are set-up. The linear set of coupling equations for the module coupling currents is determined numerically from the solutions of the tridiagonal sets of linear equations — one set for each module. The resulting set of coupling equations is then solved. This indirect procedure for solving the

linear system of equations for the loop currents permits the use of a desk-top computer, even for large numbers of cells and many modules. The reversed current for each cell is then computed, as is the charge transferred by the reversed current (eqn. (23), ref. 1). The loop currents are used to calculate the charge transferred to each cathode. Using the charges transferred during the time increment, the new cell and feed tube conductivities are calculated (eqn. (15), ref. 2). The time is advanced by the incremental amount and the calculations for the next time step are carried out using the new conductivities. This procedure results in a quasi-steady-state solution for the time dependence.

4. Results and discussion

Previously [1], we have pointed out that when a module contains only a few cells, all cells contribute to the parasitic currents. However, as the number of cells in a module increases, the centrally located cells contribute less and the involvement is shifted to the terminal cells. A similar effect is expected to govern the behavior of an assembly of modules. For this reason, calculations were carried out for modules with ten and fifty cells and the results examined against the quality control requirements. Calculations presented here, and the input data assembled in Table 1, pertain to the $Li/SOCl_2$ battery. For other systems, the procedure is the same; however, the relevant input data must be secured and the needed expressions formulated accordingly.

4.1. Scale-up effects

The effect of the battery size on the discharge characteristics is examined from two viewpoints: (i) the module size (*i.e.*, the number of cells in a module) and (ii) the battery size (*i.e.*, the number of modules in an assembly). Well fabricated modules are assumed.

As illustrated in Fig. 7, the load current increases with an increase in the number of modules. For example, scaling-up from two 50-cell modules to five 50-cell modules, discharged through the same external resistance, increased the load current by *ca.* 10%. This is an expected behavior since the increase in the number of modules reduces the discharge current density in the individual modules which, in turn, reduces their polarization.

Practically all battery systems employ porous structures; thus, their fabrication incurs statistically spread deviation in, for example, pore size, tortuosity factor, and catalytic activity. Cumulatively, this statistical variation is identified here with the porosity variation and is controlled by N_s, the fineness factor [1]. The effect of the binomial distribution of the porosity, described in Section 3.3, on the module load currents is shown in Figs. 8 - 10. It is seen that within 85% of the designed discharge time, each module delivers, uniformly, a fraction of current that is determined by the statistical aspects of the individual modules. Within the remaining 15% of the

TABLE 1

Data for modeling of intercell currents in assembly of modules

Input data		
Electrolyte conductance	κ (S cm^{-1})	0.01
Deposit conductance	κ_d (S cm^{-1})	100.0
Electrode polarization — anode	κ_a (S cm^{-2})	5.0
Electrode polarization — cathode	κ_c (S cm^{-2})	1.0
Open circuit potential	U (V)	3.74
Deposit volume (eqv.)	V_d (cm^3)	25.0
Fill tube — length	l_t (cm)	0.04
Feed path — thickness	d (cm)	0.05
Electrode separation (nominal)	δ^* (cm)	0.04
Feed path porosity (nominal)	$\epsilon_{f,n}$	0.8
Cell porosity (nominal)	$\epsilon_{z,n}$	0.5
Maximum porosity	ϵ_{max}	0.9
Minimum porosity	ϵ_{min}	0.3
Fill tube radius	r_t (cm)	0.3
Electrode inner radius	a (cm)	1.3
Electrode outer radius (eqv.)	b (cm)	8.7
Number feed tubes/module		2
Cell lifetime	τ (s)	480.0
Coupling factor	α	1.0
Number cells/module	N	50
Factor (see ref. 2)	ξ_c	13.0
Factor (see ref. 2)	ξ_f	1.0
Load resistance	R_l (Ω)	3.0

Coupling factor: $\alpha = R_{(m),(m+1)}/R_t$ with R_t given by eqn. (34) of ref. 1.

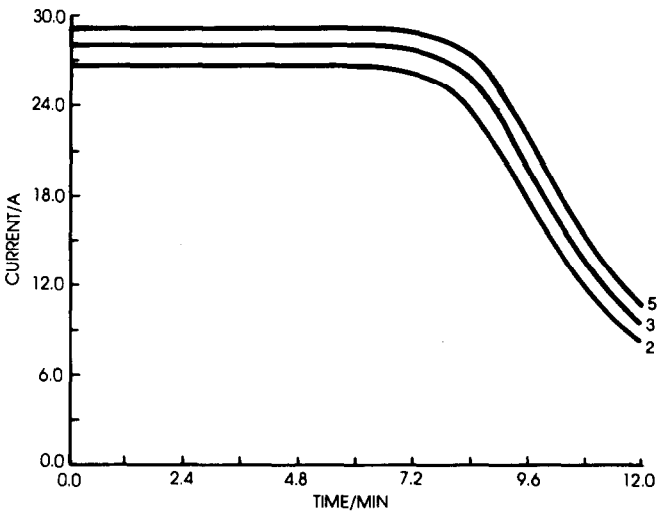

Fig. 7. External load current in an assembly of 50-cell modules with N_s = 10. The other input data are listed in Table 1. The number of modules in an assembly is indicated alongside the curves.

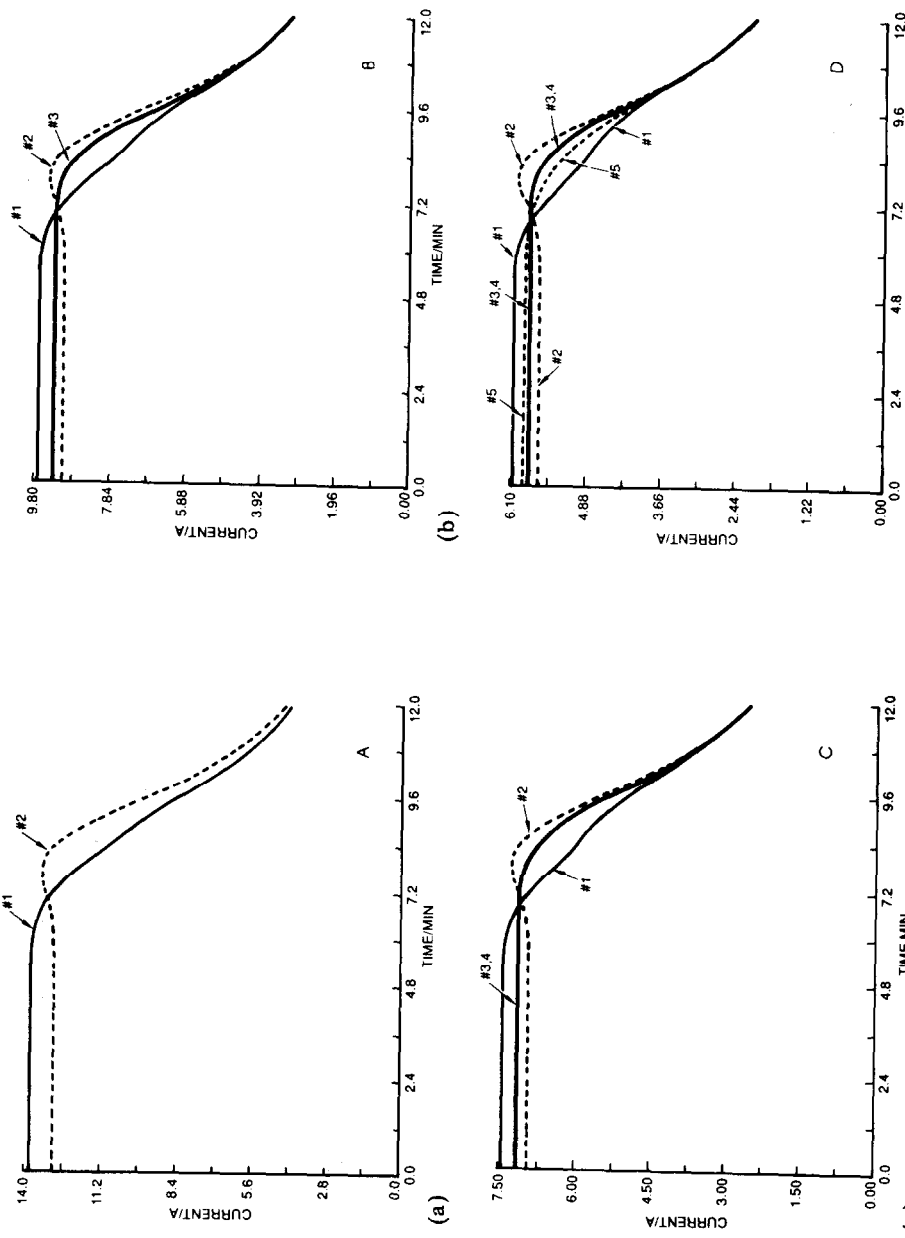

Fig. 8. Portion of load current supplied by individual modules: (a) - (d), for assemblies of 2, 3, 4, and 5 modules, respectively. Conditions as in Fig. 7.

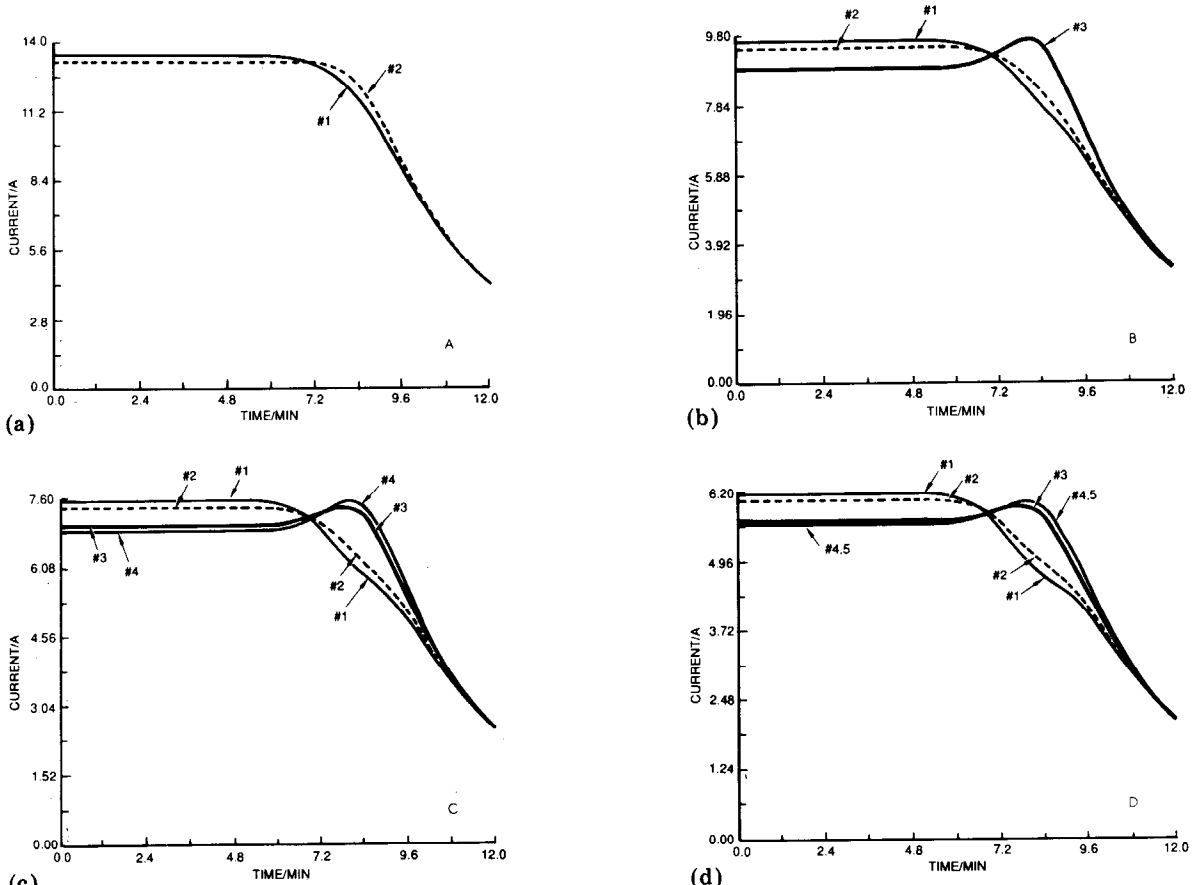

Fig. 9. Portion of load current supplied by the individual modules: (a) - (d), for assemblies of 2, 3, 4, and 5 modules, respectively. Conditions as in Fig. 7, except that $N_s = 5$.

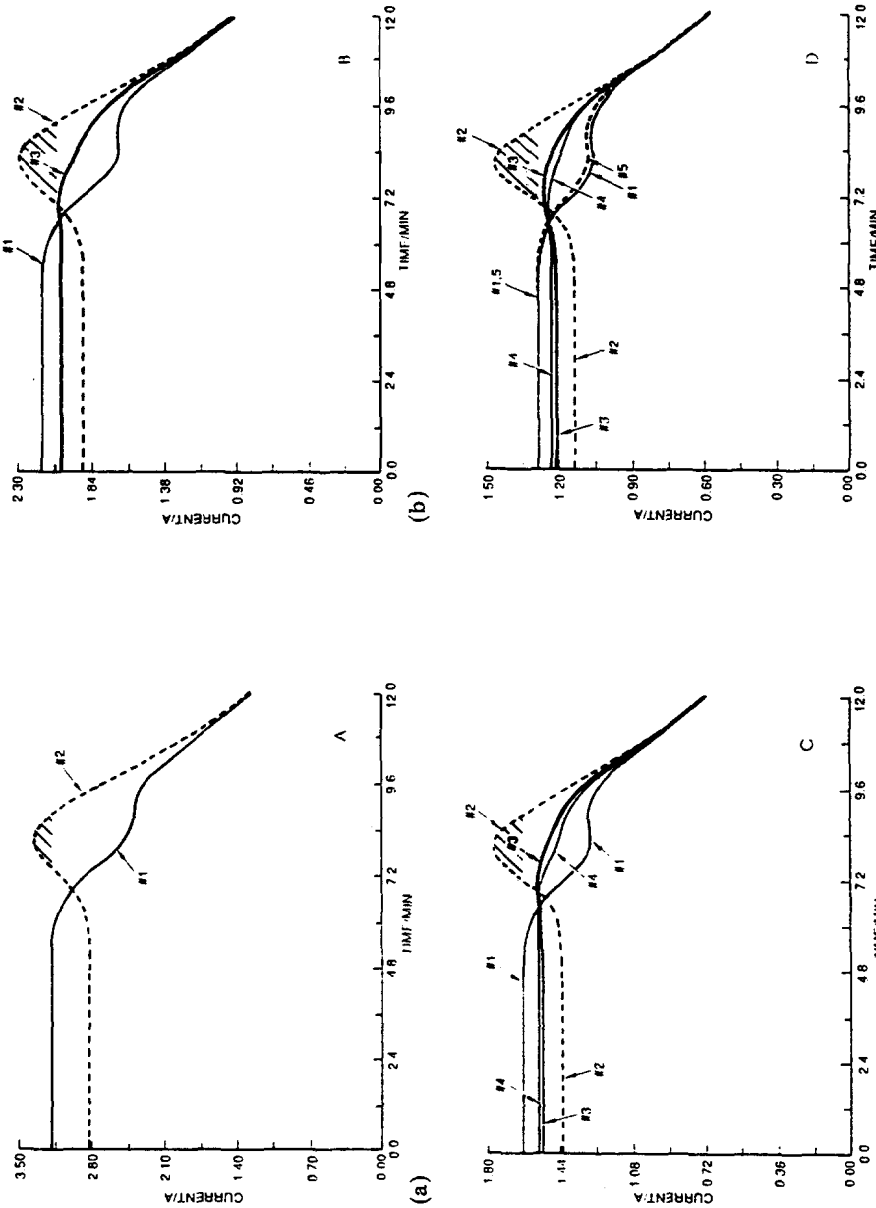

Fig. 10. Portion of load current supplied by the individual modules: (a) - (d), for assemblies of 2, 3, 4, and 5 modules, respectively. Conditions as in Fig. 7.

designed discharge time there is a clear manifestation of load sharing in which the already depleted modules deliver less current and other modules compensate by increasing their contribution, as evidenced by a cross-over of the load currents. This load sharing presents no problems if the modules contain a large number of cells. If fewer cells comprise a module, local heating may occur toward the end of discharge, as indicated by the shaded area in Fig. 10(d). Examining Figs. 9 and 10, we note that, for modules having a large number of cells, the effect of the fineness factor on the load distribution is minimal. For an assembly of modules with only a few cells, the effect is more pronounced.

4.2. Effect of variation in module compression/expansion

A typical assembly sequence is as follows: the individual cells are stacked with due attention to alignment. When a predetermined number of cells is in place, then the module is compressed to the desired thickness. In one procedure, a variation of 4% in either compression or expansion is acceptable [4]. From the QC point of view, we need to examine the effect of cell compression and/or expansion on the load current as well as currents delivered by individual modules. As expected and confirmed in Fig. 11, modules in compression, *i.e.*, decreased δ^*, contribute more to the load current than those in expansion. Our model implies that a variation of up to 10% is acceptable. It is noteworthy that the battery load current is not affected throughout the duration of the discharge. Any correlation between porosity and compression has been omitted.

4.3. Unequal numbers of cells in modules

Large $Li/SOCl_2$ power sources, *e.g.*, 10 kW, contain *ca.* 100 cells per module. This large number of cells increases the probability of constructing modules with fewer, or greater, than the specified number of cells. The effect of such an error is illustrated in Fig. 12. It is seen that missing- or additional cells in the amount of 2% affect the battery lifetime and load delivered to the external circuit. Specifically, the effect of fewer cells is similar to that resulting from an expansion in module thickness (*i.e.*, increased δ^*), while the effect of extra cells corresponds to a compression. In either case, the deficient module may generate excess heat, as illustrated in Fig. 12 by the shaded areas.

4.4. Modules with defective cells

Defective cells in a module are cells that fail prematurely. The measure of their deficiency is introduced through the computational factor w, see eqn. (3), which varies between zero and unity and affects both the conductivity in the cathode and the total charge deliverable by a cell [1]. The smaller this factor, the more serious the defect. The occurrence of these defects in the $Li/SOCl_2$ system is associated with cathode fabrication.

To illustrate the effect of defective cells in an assembly of modules, we selected central cells of the second module and assigned the deficiency

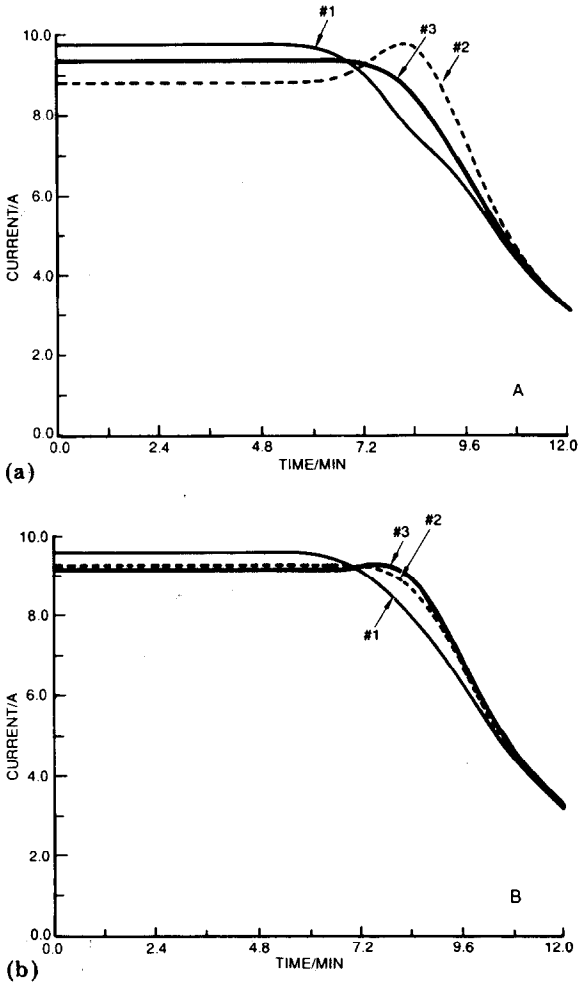

Fig. 11. Portion of load current supplied by each module in a 3-module assembly. Conditions as in Fig. 7, except for δ^*. (a) 4% compression; (b) 4% expansion.

factor $w = 0.5$. It is seen that half-way through the discharge process, the battery load current became less, Fig. 13(a), due to the failure of the first module. It is also seen that the remaining modules were unable to compensate completely, Fig. 13(b). Moreover, as illustrated in Fig. 13(c) and (d), local heat sources are generated by the intercell currents, in addition to an excessive heat production due to an increase in the load currents generated by the well functioning modules.

5. Concluding remarks

QC aspects of the fabrication of a multimodule $Li/SOCl_2$ battery employing common electrolyte are examined with regard to:

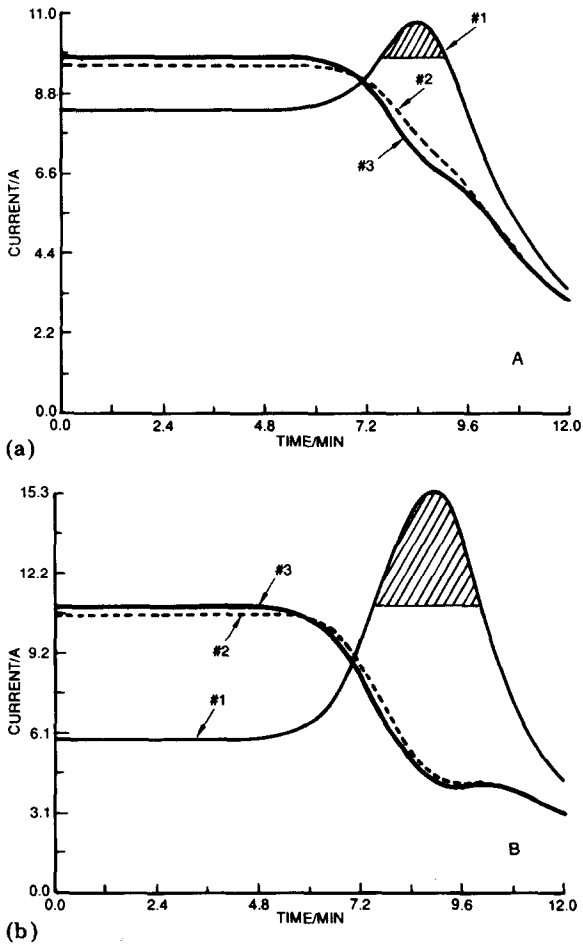

Fig. 12. Portion of load current supplied by each module in a 3-module assembly. Conditions as in Fig. 7, except for the number of cells in the first module. (a) 49 cells; (b) 48 cells.

(i) tolerances on compression and/or expansion (thickness of a module);

(ii) missing or extra cells;

(iii) the presence of defective cells.

Present calculations confirm earlier findings that the addition of well constructed modules introduces no special difficulties. Our model also predicts that tolerances in module thickness up to *ca.* 10% are acceptable. The variation in the number of cells in a module up to 2% can be tolerated. Modules with missing cells behave as if they were in expansion. The most serious problem arises from the construction of deficient cells, thus suggesting a strict enforcement of the control measures in the fabrication of positive electrodes.

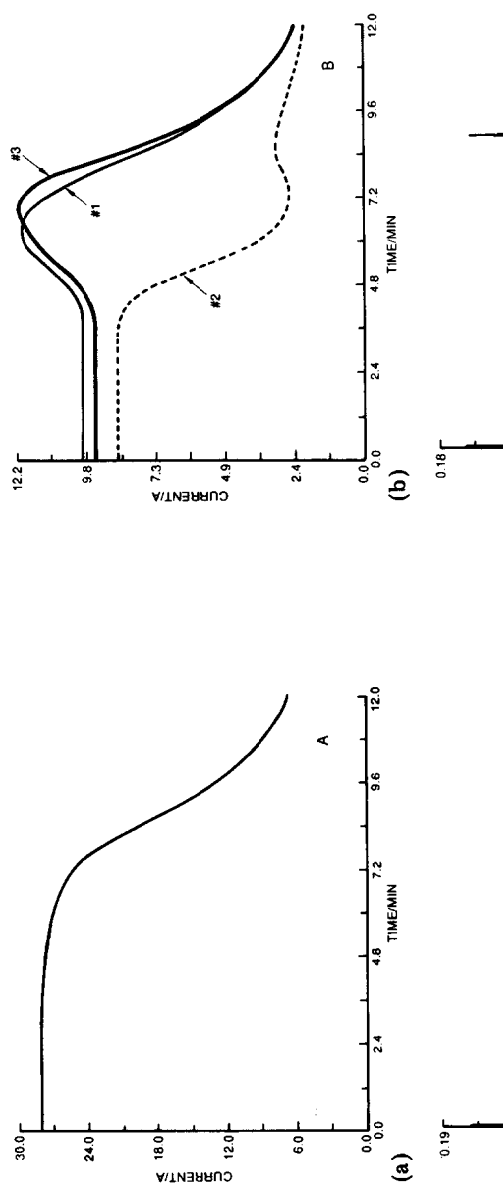

Fig. 13. Effect of a group of defective cells on battery performance. The deficient cells are numbers 29 - 32 of the second module, corresponding to numbers 69 - 72 of the complete assembly. Conditions as in Fig. 7, except that the defective cells have a deficiency factor $w = 0.5$. (a) external load current; (b) load current supplied by the individual modules. The evolution of the intercell current distribution: (c) at 4.8 min; (d) at 7.2 min.

Acknowledgement

This work was performed as a part of the Naval Ocean Systems Center Independent Exploratory Development program and constitutes a fraction of a program to establish a technology base for high discharge rate $Li/SOCl_2$ batteries.

List of symbols

i	Running index
I	Intercell current (A)
J	Current (A)
M	Number of modules in a battery
N	Number of cells in a module
R	Resistance (Ω)
t	Time (s)
w	Faradaic inefficiency factor
X	Dimensionless resistance (defined in text)
y	Random variable
δ^*	Effective distance between electrodes (cm)
ϵ	Porosity
$\epsilon_{max}; \epsilon_{min}$	see Section 3.3
Φ	Potential (V)
λ	Defined in text (eqns. (1) and (2))
η	Mean value
σ	Standard deviation

Subscripts

f	Feed line
l	Load
n	Nominal
p	Cell port entrance
t	Fill tube
z	Cell internal

Superscript

(m)	Module identification

References

1 S. Szpak, C. J. Gabriel and J. R. Driscoll, *J. Electrochem. Soc., 131* (1984) 1996.
2 S. Szpak, C. J. Gabriel, J. J. Smith and J. R. Driscoll, *J. Electrochem. Soc., 137* (1990) 849.
3 C. J. Gabriel and S. Szpak, *J. Power Sources, 25* (1989) 215.

4 S. Szpak and J. R. Driscoll, Assessment of Li/$SOCl_2$ Battery Technology: Reserve, Thin Cell Design, *NOSC-TR 1154*, Vol. I, 1987.
5 J. R. Driscoll and S. Szpak, *J. Power Sources, 14* (1985) 285.
6 J. S. Dunning, *Ph.D. Dissertation*, UCLA, 1970.
7 R. de Levie, Porous and rough electrodes, in P. Delahay and C. W. Tobias (eds.), *Advances in Electrochemistry and Electrochemical Engineering*, Vol. 6, Interscience, NY, 1967, and references therein.
8 L. A. Parnell and S. Szpak, *Electrochim. Acta, 30* (1985) 913.